Sensors & Diagnostics

PAPER

View Article Online
View Journal | View Issue

Cite this: *Sens. Diagn.*, 2024, **3**, 1984

Application of surface selective site-directed crystallization in a visual assay of DNA†

Jinrong Chen,[ab] Ruwen Xie,[a] Rui Liu, [b] Lishang Liu *[a] and Shusheng Zhang *[a]

Received 9th May 2024,
Accepted 8th October 2024

DOI: 10.1039/d4sd00149d

rsc.li/sensors

Visual analysis methods have received widespread attention due to their simplicity, economy, and intuitive results. In this work, a visual DNA quantitative analysis method based on surface selective site-directed crystallization (SSSC) was developed. Firstly, we explored the formation of calcium carbonate crystals with unique polymorphism induced by the surface of functionalized glass slides with different groups; among them, the calcite induced by the –COOH functional group has a uniform shape, larger size, and even distribution, so it serves as a signal promoter. In contrast, due to the $-N(CH_3)_3$ group acting as a signal inhibitory molecule by inhibiting crystallization, the signal molecule is captured through DNA hybridization, and the crystallization reaction is performed. The calcite growing on the DNA site is visible to the naked eye, and the DNA molecules hybridized on the surface of the glass slide are further quantified. The detection limit of this proposed visual method is 0.1 fM, and only a smartphone is needed to complete basic quantification. This work provides a basis for research into the use of single crystals as digital readouts in the field of DNA analysis, with the advantages of being simple and economical and requiring minimal equipment.

Introduction

Nucleic acid detection has become a key technology in areas ranging from disease diagnosis to environmental assays.[1–3] In the past decade, numerous detection platforms based on colorimetric, fluorescent,[4–6] Raman,[7] magnetic,[8,9] motional[10] or electrochemical transducers[11] have been developed to convert nucleic acid hybridization events into various kinds of signals. However, it remains challenging to quantify DNA molecules without costly and sophisticated instruments. Lateral flow assays have been translated from dedicated laboratory instruments into simple paper-based systems, with limited sensitivity and poor quantitative performance.[2] Visible counting strategies have received considerable attention; however, amplification-free and femtomolar sensitivity assays were only achieved by single-molecule fluorescence detection, which requires a sophisticated optical system.[4]

Digital counting strategies were developed but suffered from low sampling efficiency, complicated fabrication, and expensive equipment.[12] A variety of probes have been utilized for visible counting strategies such as bubbles, beads, and microorganisms.[13–15] Zhou *et al.* utilized T7 phages (size: ~5 μm) assembled with gold nanoparticles (GNPs) in a 'one-to-one' manner as visible probes to count the virus numbers with the naked eye.[16] They also attempted to quantify antigen molecules by counting gold nanoparticles (size: ~80 nm) assisted by scanning electron microscopy (SEM) manipulation.[17] Shlyapnikov *et al.* presented a microarray-based assay of DNA fragments using magnetic beads (size: ~1 μm) as visible signals to quantify the DNA with an electrophoresis apparatus.[18] Nam *et al.* utilized polyethyleneimine (PEI)-reduced Cu particles (size: ~100 nm) on GNPs as an amplified signal to quantify DNA molecules.[19] Tekin *et al.* tried to label protein molecules with micro-sized magnetic beads (size: ~480 nm) based on dipole–dipole-assisted interaction.[20] Tam *et al.* attempted to increase the size of AuNPs *in situ* after labeling protein molecules.[21] Wang *et al.* designed a method to capture the target proteins using antigen-labeled paramagnetic microspheres, which were further combined with PtNPs to produce quantifiable microbubbles (size: >35 μm) in response to H_2O_2.[22] Transferring the invisible biomolecule information into visual probes, which are directly countable, is the most cost-effective method. However, it's challenging to directly label biomolecules with visible particles.

Surface-induced selective crystallization has been studied and applied in drug separation and purification, polymorphism discrimination, and rare earth element

[a] *Shandong Province Key Laboratory of Detection Technology of Tumor Markers, Linyi University, Linyi 276005, China. E-mail: liulishanghao@126.com, shushzhang@126.com*
[b] *Department of Biotechnology, College of Engineering, The University of Suwon, Hwaseong 18323, Korea*

† Electronic supplementary information (ESI) available. See DOI: https://doi.org/10.1039/d4sd00149d

separation.[23] In template-induced nucleation, crystal growth shifts molecular recognition to the nucleation stage. In our previous work, the selective crystallization of $CaCO_3$ at specific sites was analyzed by quartz crystal microbalance (QCM).[24,25] The bulk crystals generated on the surface of the QCM sensor act as amplifiers, clearly improving the sensitivity of the mass sensor. Crystals can be quantitatively controlled by tightly controlling the ratio of inhibitor and promoter groups. In fact, the reduction of silver ions to silver in the work of Zhou *et al.* is similar.[1] Group-induced crystals have high potential for application as quantitative molecular indicators.

To demonstrate this capability, in this work, we propose a DNA hybridization assay method based on surface selective site-directed crystallization (SSSC) as shown in Scheme 1. First, the selective crystallization of different forms of $CaCO_3$ crystals is realized on the surface of functionalized glass slides, and $-N(CH_3)_3$ is determined to be the signal inhibitory group and –COOH as the signal promoter. Capture DNA (cDNA) is introduced on the surface of the glass slide. When the target DNA (tDNA) is present, it can hybridize with the DNA labeled by the signal promoter (pDNA) and promote the site-specific crystallization of calcite. The target molecules are visualized and detected by observing the crystals, while quantitative detection is achieved by counting calcite crystals using simple optics and smartphones. Therefore, the DNA hybridization strategy proves the selective crystallization and *in situ* crystallization ability of crystals as quantitative analysis probes. The method is simple to operate and does not require major instruments, and the results are visible to the naked eye. This work uses single crystals as quantitative signals for analysis and detection, providing new ideas for analysis and research workers.

Materials and methods

Reagents and equipment

Bacillus anthrax (BA) human immunodeficiency virus (HIV) and hepatitis B virus (HBV) DNA oligonucleotides were from Sangon Biotech, and they are listed in Table S1.† Glass slides (25 mm × 75 mm) were from Thermo Scientific. $HS(CH_2)_{15}$-COOH, $HS(CH_2)_{11}OH$, $HS(CH_2)_{11}CH_3$, and $HS(CH_2)_{11}NH_2$ were purchased from Sigma-Aldrich. $HS(CH_2)_{11}N(CH_3)_3Cl$ was purchased from Prochimia. $CaCl_2{\cdot}2H_2O$, $(NH_4)_2CO_3$, tris(2-carboxyethyl) phosphine hydrochloride (TCEP) and bovine serum albumin (BSA) were purchased from Aladdin. Absolute ethanol, sulfuric acid, ammonia solution, and dimethyl sulfoxide were purchased from Shanghai Chemical Reagent Co. Ltd. Hydrogen peroxide and acetic acid were purchased from Sinopharm Chemical Reagent Co. Ltd. 3-(2-Aminoethylamino)propyltrimethoxysilane (EDA) was purchased from Alfa Aesar Co. Succinimidyl 4-(*N*-maleimidomethyl)cyclohexane-1-carboxylate (SMCC) was purchased from Shanghai MERYER Co. All aqueous solutions were prepared using ultrapure water (Milli-Q, Millipore).

$CaCO_3$ crystals were characterized by SEM (JSM-7610F), Raman (Renishaw), X-ray diffraction, and optical microscopy (ECLIPSE Ni-U). Confocal images were obtained using a Nikon 6CR609WPQV. A 20× to 200× universal tipscope was purchased from TMALL. A 20× to 400× tipscope was purchased from Jing Dong.

Preparation of glass glides

Glass slides were first treated with a freshly made piranha solution (hydrogen peroxide : concentrated sulfuric acid = 3 : 1, v/v) at 90 °C for 2 h and thoroughly rinsed with deionized water. The glass slides were allowed to react with EDA in an acetic acid solution (EDA : 1 mM acetic acid = 1 : 100, v/v) at room temperature for 30 min, followed by washing three times in deionized water, drying with nitrogen, and then baking at 120 °C for 30 min. The glass slides were immersed in a 5 mM DMSO : ethanol (2 : 3, v/v) solution of a bifunctional coupling reagent, SMCC, overnight and then were washed in ethanol and water, and dried with nitrogen. Functional groups were formed on glass slides (Fig. S1†) by exposing the surfaces to a 10 mM solution of thiol in ethanol for 12 hours, followed by washing with ethanol and drying with nitrogen gas.

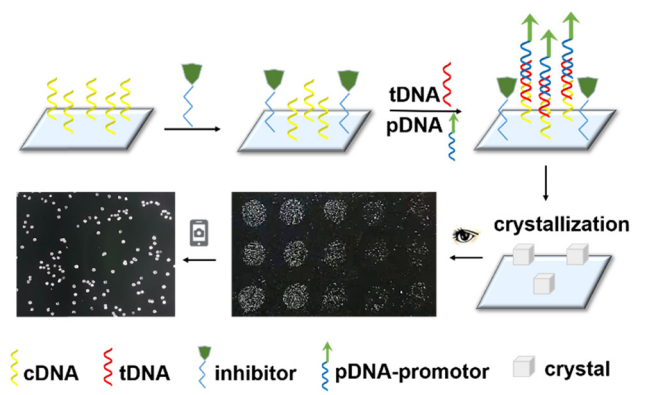

Scheme 1 Scheme of the surface selective site-directed crystallization DNA assay method.

Preparation of the hybridization sandwich

The cDNA-immobilized glass slides were obtained by spotting 5 μL of 1 nM cDNA solution (buffer: 0.02 M PBS, 0.25 M NaCl, pH 7.4) for 8 hours at 37 °C, followed by blocking with 10 mM $HS\text{-}C_{11}\text{–}N(CH_3)_3Cl$ for 12 hours and rinsing three times with a washing buffer (1 × SSC + 0.1% (v/v) SDS). The prepared glass slides were stored at 4 °C. tDNA of varied concentrations (5 μL solution with buffer: 0.02 M PBS, 0.25 M NaCl, pH 7.4) was hybridized with cDNA immobilized on the surface of the slides. Further hybridization with pDNA (5 μL, 1 nM) was carried out. After each step, the slide was washed in a washing buffer and deionized water to remove non-hybridization DNA, and then dried with nitrogen gas.

Promoter optimization

SMCC treated glass slides were exposed to a 10 mM thiol solution ($HS(CH_2)_{15}COOH$, $HS(CH_2)_{11}OH$, $HS(CH_2)_{11}NH_2$, or $HS(CH_2)_{11}N(CH_3)_3Cl$) in ethanol for 12 hours, followed by washing with ethanol and drying with nitrogen gas. The prepared glass slides were placed upside down and the crystallization experiment was conducted.

Inhibitor optimization

SMCC treated glass slides were first modified with cDNA (100 nM, 10 nM, 1 nM, 100 pM, 10 pM, or 1 pM) and then immersed in an inhibitor solution (10 mM $HS(CH_2)_{11}CH_3$, 10 mM $HS(CH_2)_{11}N(CH_3)_3Cl$, or 1% BSA) for 12 hours, followed by washing in ethanol and drying with nitrogen gas. The prepared glass slides were placed upside down and the crystallization experiment was conducted.

Crystallization of $CaCO_3$ on the glass slide surface

The prepared glass slides were placed upside down, emerged in calcium chloride solution, surrounded with solid ammonium carbonate in a beaker, then sealed and reacted at room temperature. Finally, the slides were washed in deionized water and dried with nitrogen gas.

The crystals on the glass slides were observed by optical microscopy and SEM, and the morphology, number, and size of the crystals on the glass surface were recorded. The crystals on the glass slides were characterized by Raman and XRD to confirm their polymorph.

Calibration of the SSSC assay

After hybridization, the glass slides were placed upside down in a flask containing 3 mM calcium chloride solution, surrounded with solid ammonium carbonate. The reaction device was sealed and placed under an optical microscope (20×) to observe and record the crystallization process in real time.

The crystallized glass slide was photographed on a black background with a smartphone using an attached tipscope (microscope). The crystals were counted using Image J or the "Count Things" application on the phone. The CV of the crystal number against counting area (take the result of 1 pM tDNA as an example) was analyzed.

The specificity of the DNA assay

Solutions of 1 nM target BA sequence, HIV, HVB, and random sequences were tested by the SSSC assay.

Results and discussion

Rationale of the SSSC assay method

Templated heterogeneous nucleation is driven by the characteristics of the templates, including topography, surface functionality, and lattice matching between the crystal and substrate, favoring the directional growth of the crystal. In this work, a glass slide was used as a substrate for the perspective disposal device. The site-specific crystallization was carried out on a glass slide surface for perspective disposal devices. Selective crystallization of $CaCO_3$ on self-assembled monolayer (SAM) modified gold surfaces has been researched;[26] however, that on glass slides has rarely been reported even though glass slides have commonly been applied in biological imaging.[27,28] Therefore, the modification of the glass slide surface was optimized to select the best inhibitor and promoter for the site-specific crystallization and finally to guarantee the uniformity and discreteness of the generated crystals.

In the DNA hybridization assay, as shown in Scheme 1, after immobilization of capture DNA (cDNA) on the slide surface, a layer of inhibiting group was introduced to prevent nonspecific crystallization. Upon the hybridization of the target DNA, probe DNA (pDNA) with a promoter group hybridized further as a specific site for crystallization. The *in situ* crystallization reaction was carried out by placing glass slides inversely in calcium chloride solution with gas diffusion. The inversion of glass slides can avoid nonspecific crystal settling. Therefore, only in the presence of target DNA can the crystals grow and be visualized. Then, the visual detection of the target can be achieved, and its quantification can be further achieved by crystal counting.

Surface induced acceleration of $CaCO_3$ crystallization

$CaCO_3$ crystallizes in three polymorphs: calcite, aragonite, and vaterite. However, the polymorphic control of $CaCO_3$ crystals was not deeply investigated. Studies of templated $CaCO_3$ nucleation on metal SAM surfaces concluded that –COOH, $-PO_3^{2-}$, and –OH groups were active in facilitating nucleation, while $-N(CH_3)_3^+$ and $-CH_3$ inhibited nucleation. The type of nucleation of $CaCO_3$ induced by –COOH and –OH was oriented, while that induced by $-PO_3^{2-}$ was random.[29] As $-NH_2$ is also a common label in DNA sensing, to select the best crystal candidate as a visual probe for site-specific $CaCO_3$ nucleation, we tested glass slides modified with –COOH, $-NH_2$, –OH functional groups and analyzed the polymorph, morphology, and size distribution of the generated crystals. The morphological results were shown by SEM (Fig. 1) and their polymorphism was demonstrated by XRD and Raman (Fig. S2 and S3†) and the optical microscopy images in Fig. S4.† The polymorphic fraction and coefficient of variation (CV) of size distribution are summarized in Table 1. Rhombohedral and pumpkin-shaped crystals with random size were observed on the $-NH_2$ terminated slide surface and proved to be calcite and vaterite, respectively, with a CV of the crystal size of ~60%.

Cubic calcite crystals were exclusively obtained on the –COOH terminated surface. Their strong and sharp XRD peaks indexed to the (104) plane (Fig. S2†) confirmed the excellent crystallization of calcites. All the calcite crystals on the –COOH terminated surface were found to be "standing" on the slide surface with a uniform orientation. Significantly,

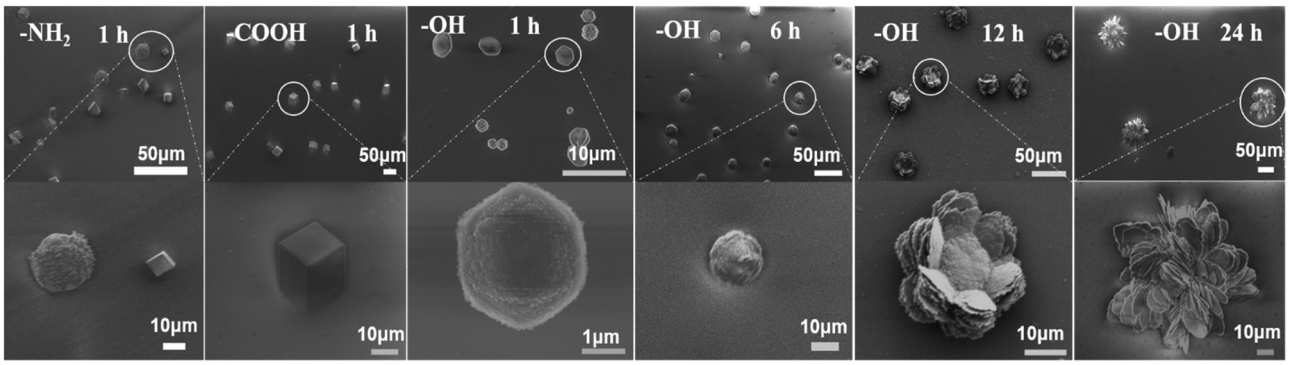

Fig. 1 SEM characterization of crystals formed on functionalized slide surfaces. A mixture of pumpkin-shaped and rhombohedral crystals was found on the $-NH_2$ terminated surface. Uniform cubic crystals were found on the –COOH terminated surface. Thick plate-shaped (1 h), pumpkin-shaped (6 h), lotus-shaped (12 h) and flower-shaped (24 h) crystals were found on the –OH terminated surface.

Table 1 The uniformity analysis of $CaCO_3$ crystals generated on functionalized surfaces

Surface group	Proportion of calcite	Proportion of vaterite	Number of crystals	Crystal size (μm)	CV of crystal size
$-NH_2$	86%	14%	~80	5–30	60%
–COOH	100%	0	~120	10–25	19%
–OH (t_c: 1 h)	8%	92%	~80	5–15	43%
–OH (t_c: 6 h)	16%	84%	~70	10–20	32%
–OH (t_c: 12 h)	15%	85%	~60	5–20	30%
–OH (t_c: 24 h)	11%	89%	~50	5–50	32%

the calcite crystals were discretely distributed with a unified cubic morphology and unified size (coefficient of variation (CV) ~ 19%), and even with a unified orientation. The negatively charged –COOH group has been reported to facilitate the crystallization of calcite and influence its growth direction.[30] The main driving force for the orientation of calcite on the –COOH terminated surface is believed to be the strong interaction between the deprotonate carboxyl group and calcium ions, providing a high local supersaturation microenvironment.

The crystals generated on the –OH modified glass were more complicated. Crystals with random shapes were observed and were dominant at different crystallization times: hexagonal plate, pumpkin, hexagonal lotus, and flower. They were demonstrated to be vaterite crystals with characteristic XRD peaks of the (110), (112), (114), (104), (300), and (224) planes (Fig. S2†). The calcite crystals on the –COOH terminated surface with a unified morphology, size and orientation showed satisfactory characteristics and were believed to be an ideal candidate as a visual probe. Therefore the –COOH group was determined as the promoter group for site-specific crystallization in visual detection of DNA.

Surface inhibition of determination of $CaCO_3$ crystallization

For DNA hybridization on the substrate surface, non-specific adsorption is always prevented by further surface modification after cDNA immobilization. Functional groups such as $-N(CH_3)_3$, $-CH_3$ and –OH and bovine serum albumin (BSA) have also been reported to work as blockers of non-specific nucleic acid, protein, and other biomolecules.[29,31] In this work, the blocking of both non-specific nucleic acid and unwanted crystals is critical. The SEM pictures in Fig. 1 showed that the –OH group induced vaterite crystal growth; thus, the –OH group is not a suitable inhibitor candidate. $-N(CH_3)_3$, $-CH_3$, and BSA were further modified on a cDNA immobilized slide surface and then a crystallization experiment was introduced on the slide surface. The results are shown in Fig. 2; the $-N(CH_3)_3$ group had the best inhibitory effect probably due to repulsive forces against Ca^{2+} ions, while $-CH_3$ and BSA did not inhibit the crystallization on the cDNA immobilized slide surface. No crystal was found on the $-N(CH_3)_3$ terminated surface even with a high cDNA concentration (10 nM). Therefore, the $-N(CH_3)_3$ group was

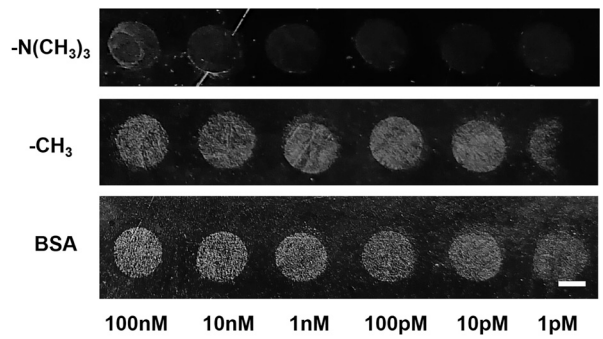

Fig. 2 Inhibition effect of $-N(CH_3)_3$, $-CH_3$ and BSA on surface crystallization cDNA concentration: 100 nM, 10 nM, 1 nM, 100 pM, 10 pM, and 1 pM. Scale bar: 2 mm.

selected and used as an inhibitor on the slide surface preventing non-specific nucleation.

In addition, QCM was used to verify whether fixing the inhibitory group and increasing the concentration of the carboxyl group could achieve the regulation of the crystal yield (Fig. S5†). The experimental results show that with the increase of carboxyl group concentration, the number of crystals increases and the QCM signal decreases, and the concentration of the carboxyl group is linearly related to the crystal quality signal. This result proves that precise crystal control can be achieved by controlling the amounts of functional groups.

Application of selective crystallization on DNA hybridized sites

Using the DNA sandwich hybridization shown in Scheme 1, $-N(CH_3)_3$ as the crystallization inhibitor and COOH as the crystallization promoter, the feasibility of the SSSC DNA assay method was tested. As designed, if no target exists, surface nucleation of $CaCO_3$ would be inhibited by the $-N(CH_3)_3$ group, and a clear surface would be observed; if target DNA exists, the –COOH group on pDNA would trigger the site-specific crystallization and a certain amount of calcite crystals would be observed.

The inhibitive group $-N(CH_3)_3$ and the promoter group –COOH in this design scheme are competitive and balancing in the crystallization process. To achieve the best DNA hybridization differentiation within a certain range, we used *Bacillus anthracis* DNA analysis as a model and optimized the experimental conditions for the SSSC method. The temperature of the DNA hybridization reaction on the glass sheet, the concentration and the time of the crystallization reaction were optimized. According to the results (Fig. S6–S8†), the DNA hybridization temperature in the subsequent SSSC DNA detection method was determined to be 45 °C, the Ca^{2+} concentration and crystallization time were 3 mM Ca^{2+} and 1 h, and the target DNA concentration ranged from 1 nm to 1 fM. At the same time, we also used fluorescence labelled DNA to verify the feasibility of the hybridization reaction on the glass slide. As shown in Fig. S9,† laser confocal microscopy can photograph fluorescently labelled DNA modified on the glass slide, which proves that the hybridization reaction on the glass slide is successful, but this result can only detect DNA of 1 μM.

The site-specific crystallization process on the DNA (100 fM) hybridized surface was observed *in situ* using optical microscopy (Fig. 3a). Before nucleation took place, the slide surface was clear. As time went by, tiny dots started to appear at the 25th min, and then crystals were found to grow at the same spots from the 30th min to 60th min, only with size increasing. The real time site-specific crystallization was recorded in a video (Video S1 in the ESI†). Together with the crystal size plot over time in Fig. 3b, it was clear that new crystals were not generated after the 36th min, and only an increase in the size of existing crystals was observed. These results demonstrated that the crystals are generated by preferred site-specific heterogeneous nucleation, not by random growth, nor by the attachment of crystals from the bulk solution. The size of the crystals is increased gradually to ~40 μm in an hour. According to this result, as visual signals, calcites can readily be observed and quantified.

The cooperation of the inhibitor and promoter guaranteed the selective nucleation of crystals. The SEM pictures of crystals with increasing DNA concentration are shown in Fig. 4. These pictures and XRD analysis patterns (Fig. S10†) again confirmed that the $CaCO_3$ crystals obtained are discrete and uniform in size and morphology, indicating that the nucleation is highly restricted. The binding of Ca^{2+} ions to –COOH groups can increase the nucleation rate of $CaCO_3$ crystals by increasing the local supersaturation ratio of $CaCO_3$ molecules. The –COOH here works as a "spear" to catch Ca^{2+} ions, and it also plays a key role in the regulation of polymorphism, morphology, size, and direction of the crystal. The obtained calcite crystals show perfect discreteness and can be easily enumerated. These properties make calcite crystals ideal quantitative probes, so it is feasible to transfer the detection of DNA hybridization by calcite crystal counting schemes.

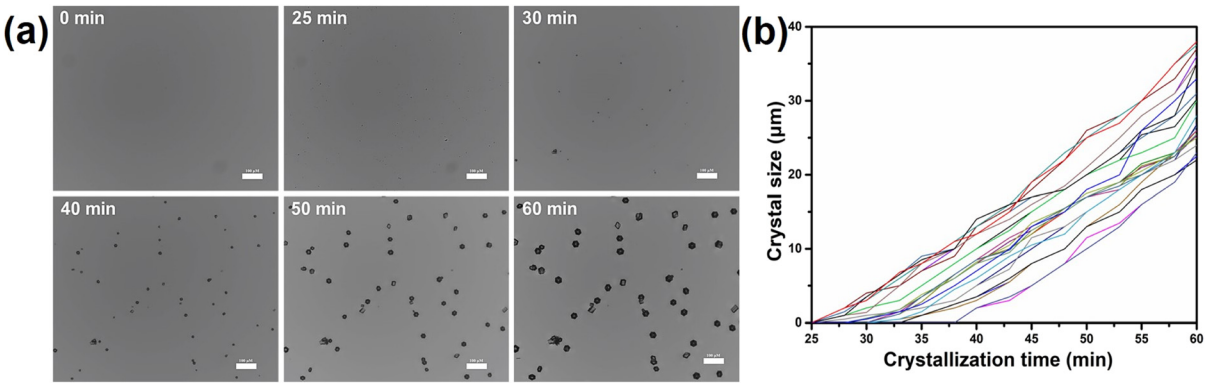

Fig. 3 (a). *In situ* optical microscopy images of 100 fM tDNA site-specific nucleation of calcites with crystallization time: 0 min, 25 min,30 min, 40 min, 50 min, and 60 min (scale bar: 100 μm); (b). The size of nucleated crystals increased with time.

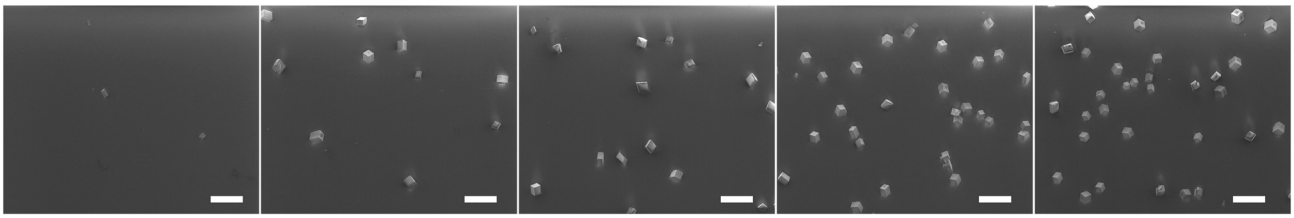

Fig. 4 SEM characterization of the slide surface in the SSCV DNA assay. Calcites are uniformly distributed and their quantity increases with the increment of tDNA concentration: 0 M, 1 fM, 10 fM, 100 fM, and 1 pM (scale bar: 100 μm).

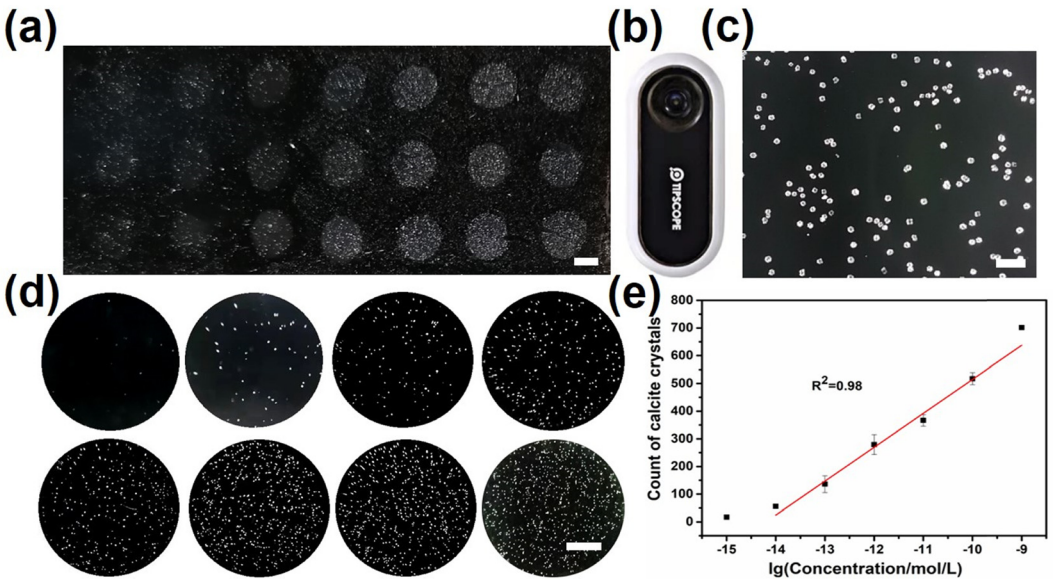

Fig. 5 (a): Smartphone images of slide surfaces in the DNA assay (1 fM, 10 fM, 100 fM, 1 pM 10 pM, 100 pM, 1 nM), scale bar: 2 mm. (b and c): A 20× to 400× universal tipscope and smartphone image, scale bar: 100 μm. (d) Smartphone images using a 20× to 200× tipscope with DNA concentrations of 0 M, 1 fM, 10 fM, 100 fM, 1 pM, 10 pM, 100 pM, and 1 nM, scale bar: 1 mm. (e) Calibration curve of site-specific crystallized calcites with DNA concentration (mean ± standard deviation; n = 3).

Calibration of the crystal amount induced by DNA hybridization

The results of the analysis of different concentrations of tDNA are shown in Fig. 5a. Next, crystals of DNA sites were quantified using a smartphone. A universal tipscope was attached to a smartphone to take photos (Fig. 5b and c and S11†). The pictures in Fig. 5d were sent to Image J to count the number of calcite crystals. To explore the effect of the sampling area on the counting results, the coefficient of variation (CV) of the number of crystals is plotted against the area in Fig. S12.† As the detection area increased, the CV decreased, so we counted the crystals in the entire puncta area to reduce sampling error. To achieve quantitative analysis more easily, the smartphone app "Count Things" was also used to count the crystals. Examples of smartphone application interfaces are shown in Fig. S13.† Similar enumeration results were obtained using ImageJ and "Count Things" (Fig. S14†). The numbers of crystals were counted over three repeats of results of experiments and found to be positively correlated with the concentration of target DNA, as shown in Fig. 5e. The linear regression follows the equation $Y = 122.5X + 1739.4$ with an R^2 of 0.98. The linear range of the SSSC DNA assay method is from 1 nM to 10 fM, and the limit of detection (LOD) is calculated to be 0.1 fM.

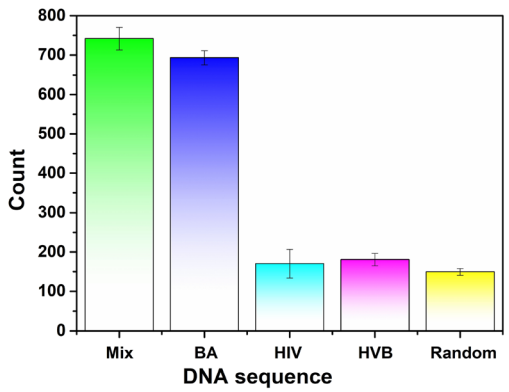

Fig. 6 The specificity of the SSSC DNA assay method (the concentration of sequences: 1 nM, mean ± standard deviation; n = 3).

Table 2 Comparison of quantitative detection methods of particle counting

Detection method	Target	Signal	Particle size	Linear range	LOD	Instrument	Ref.
Magnetic bead surface coverage assay	Protein	Magnetic beads	2.8 μm	1–1 × 10^8 pg mL^{-1}	1 pg mL^{-1}	Required	20
Phage-mediated counting	miRNA	Phages	~1 μm	0.2–0.01 fM	0.003–0.005 fM	Required	16
Multiplex microarray-based assay	DNA	Magnetic beads	1 μm	1000–0.1 fM	0.1 fM	Required	18
Simple microbubbling digital assay	Protein	Microbubbles	35–100 μm	0.06–1 pg mL^{-1}	0.06 pg mL^{-1}	Not required	22
Dropcast single-molecule assays	Protein	Paramagnetic beads	2.7 μm	10–3 – 102 fM	0.0192 fM	Required	12
Pre-equilibrium digital ELISA	Protein	Magnetic beads	~4 μm	40–1000 pg mL^{-1}	25.9 pg mL^{-1}	Required	32
SSCV	DNA	Calcite	20–40 μm	1 nM–1 fM	0.1 fM	Not required	This work

Finally, we investigated the specificity and reproducibility of the method. To evaluate the reproducibility of our method, we analyzed the CV of the calcite number in the SSSC DNA assay. It is summarized in Table S2,† with an average value as small as 11%, indicating that the reproducibility of this method is good. The specificity of our approach was investigated using several different DNA sequences (Fig. 6). It could be seen that 1 nm BA DNA and mixed sequences can produce strong signals, while the other DNA sequences (HIV, HVB, and random sequence) cannot show significant signals. This indicates that the method has good specificity.

Conclusions

In conclusion, this study established a visual DNA quantification method by surface-selective site-specific crystallization and counting calcite crystals. DNA site-induced calcite crystals have been shown for the first time to serve as signal probes to amplify the microscopic world. The crystals obtained were all calcite, and the uniformity of their polymorphic forms and growth directions suggested that they were induced specifically by hybridization of the target DNA rather than randomly.

The single calcite crystals crystallized at the site are uniform in size, shape, and distribution. Compared with the reported visible probes such as magnetic beads, bacteriophages, copper particles, and bubbles, calcite crystals have the advantages of low cost and high stability, making them ideal visual digital probes. Compared with previously reported studies also based on visual particle counting (Table 2), the calcite crystal counting method proposed in this work demonstrated a wide linear range without the aid of any professional instruments. Notably, quantitative analysis can be achieved using a smartphone in conjunction with a portable microscope. This method has the advantages of simple operation and no need for amplification, which opens a new route for the design of visual sensors.

Data availability

The data supporting this study's findings are available from the corresponding author upon reasonable request.

Author contributions

The manuscript was written through the contributions of all authors. All authors have approved the final version of the manuscript.

Conflicts of interest

There are no conflicts to declare.

Acknowledgements

This work was supported by the National Natural Science Foundation of China (21675076, 81502585, 22076073).

Notes and references

1 L. Yan, J. Zhou, Y. Zheng, A. S. Gamson, B. T. Roembke, S. Nakayama and H. O. Sintim, *Mol. BioSyst.*, 2014, **10**, 970–1003.
2 M. Zhang, J. Ye, J. S. He, F. Zhang, J. Ping, C. Qian and J. Wu, *Anal. Chim. Acta*, 2020, **1099**, 1–15.
3 L. Zhang, B. Ding, Q. Chen, Q. Feng, L. Lin and J. Sun, *TrAC, Trends Anal. Chem.*, 2017, **94**, 106–116.
4 M. Di Antonio, A. Ponjavic, A. Radzevicius, R. T. Ranasinghe, M. Catalano, X. Zhang, J. Shen, L. M. Needham, S. F. Lee, D. Klenerman and S. Balasubramanian, *Nat. Chem.*, 2020, **12**, 832–837.
5 J. H. Hwang, S. Park, J. Son, J. W. Park and J. M. Nam, *Nano Lett.*, 2021, **21**, 2132–2140.
6 A. S. Law, L. C. Lee, K. K. Lo and V. W. Yam, *J. Am. Chem. Soc.*, 2021, **143**, 5396–5405.
7 F. Gao, J. Lei and H. Ju, *Anal. Chem.*, 2013, **85**, 11788–11793.
8 Z. Zhou, Y. Zhang, M. Guo, K. Huang and W. Xu, *Biosens. Bioelectron.*, 2020, **167**, 112475.
9 M. Bao, E. Jensen, Y. Chang, G. Korensky and K. Du, *ACS Appl. Mater. Interfaces*, 2020, **12**, 43435–43443.
10 X. Yu, Y. Li, J. Wu and H. Ju, *Anal. Chem.*, 2014, **86**, 4501–4507.
11 E. O. Blair and D. K. Corrigan, *Biosens. Bioelectron.*, 2019, **134**, 57–67.
12 C. Wu, P. M. Garden and D. R. Walt, *J. Am. Chem. Soc.*, 2020, **142**, 12314–12323.
13 M. G. M. Xiong Ding, K. Yin, K. Kadimisetty and C. Liu, *Anal. Chem.*, 2018, **91**, 655–672.

14 C. M. S. Hsin-I Peng, K. E. Leach, T. D. Krauss and B. L. Miller, *ACS Nano*, 2009, **3**, 2265–2273.
15 H. Xu, J. Shen, C. T. Yang, B. Thierry, Y. Zhu, C. B. Mao and X. Zhou, *Mater. Today Adv.*, 2021, **10**, 100122.
16 X. Zhou, P. Cao, Y. Zhu, W. Lu, N. Gu and C. Mao, *Nat. Mater.*, 2015, **14**, 1058–1064.
17 X. Zhou, C. T. Yang, Q. Xu, Z. Lou, Z. Xu, B. Thierry and N. Gu, *ACS Appl. Mater. Interfaces*, 2019, **11**, 6769–6776.
18 Y. M. Shlyapnikov, E. A. Malakhova and E. A. Shlyapnikova, *Anal. Chem.*, 2019, **91**, 11209–11214.
19 J. H. Kim, J. E. Park, M. Lin, S. Kim, G. H. Kim, S. Park, G. Ko and J. M. Nam, *Adv. Mater.*, 2017, **29**, 1702945.
20 H. C. Tekin and M. Cornaglia, *Lab Chip*, 2013, **13**, 1053–1059.
21 S. C. Tam, Y. H. Cheng, C. N. Lok, H. Y. Au-Yeung, W. X. Ni, X. L. Wei and K. M. Ng, *Analyst*, 2020, **145**, 6237–6242.
22 H. Chen, Z. Li, L. Zhang, P. Sawaya, J. Shi and P. Wang, *Angew. Chem., Int. Ed.*, 2019, **58**, 13922–13928.
23 F. Artusio and R. Pisano, *Int. J. Pharm.*, 2018, **547**, 190–208.
24 L. S. Liu, C. Wu and S. Zhang, *Anal. Chem.*, 2017, **89**, 4309.
25 C. Wu, Z. Sun and L. S. Liu, *Analyst*, 2017, **142**, 2547–2551.
26 H. Deng, X. C. Shen, X. M. Wang and C. Du, *Front. Mater. Sci.*, 2013, **7**, 62–68.
27 A. M. Travaille, L. Kaptijn, P. Verwer, B. Hulsken, J. A. A. W. Elemans, R. J. M. Nolte and H. van Kempen, *J. Am. Chem. Soc.*, 2003, **125**, 11571–11577.
28 H. Deng, X. M. Wang, C. Du, X. C. Shen and F.-Z. Cui, *CrystEngComm*, 2012, **14**, 6647–6653.
29 J. Aizenberg, A. J. Black and G. M. Whitesides, *J. Am. Chem. Soc.*, 1999, **121**, 4500–4509.
30 J. Aizenberg, *Adv. Mater.*, 2004, **16**, 1295–1302.
31 J. A. Y. J. Han, *J. Am. Chem. Soc.*, 2003, **125**, 4032–4033.
32 Y. Song, E. Sandford, Y. Tian, Q. Yin, A. Kozminski, S. Su, T. Cai, Y. Ye, M. Chung and R. Lindstrom, *The Journal of the American Society of Hematology*, 2021, **137**, 1591–1602.